A MODIFIED MODEL BASED SAR TARGET DECOMPOSITION METHOD FOR POLARIMETRIC DATA

Zili Shan[(1) (2)], Hong Zhang[(1)*], Chao Wang[(1)], Fan Wu[(1)], Bo Zhang[(1)], Yixian Tang[(1)]

[(1)]Center for Earth Observation and Digital Earth , CAS, No. 9, Deng Zhuang Nan Road, Haidian District, Beijing, 100094, China,
[(2)]Graduate University of Chinese Academy of Sciences, 19 A Yu Quan Road, Beijing, 100049, China,
Email: hzhang@ceode.ac.cn

ABSTRACT

This paper deals with the problems of the negative powers and the overestimated volume scattering power of the Yamaguchi Decomposition, when applied to the urban areas. Three measures, namely the orientation angle compensation, a modified volume scattering model and two power constraints are appended in our algorithm. A RADARSAT-2 quad polarimetric image acquired over the Suzhou City in China is analyzed in the experiments. Experimental results verify the effectiveness of the proposed decomposition.

1. INTRODUCTION

One of the most popular classes of the polarimetric decomposition methods for SAR data, such as the Freeman Decomposition [1], and the Yamaguchi Decomposition [2]-[3], are based on physical scattering models of microwaves. In these algorithms, the covariance or the coherency matrix is separated into several basic models corresponding to different physical scattering mechanisms in the real world. However, in applications to the urban areas, negative values will occur in the surface or the double-bounce scattering power. Additionally, many pixels are decomposed as "green", i.e., the volume scattering power is overestimated in these areas. As the Yamaguchi decomposition is a generalization of the Freeman Decomposition, we will propose a four-component decomposition to deal with these problems in this paper.

2. ANALYSES OF THE PROBLEMS

As shown in (1), in the Yamaguchi Decomposition, the coherency matrix is decomposed as a weighted sum of four types of scattering models, namely the surface scattering, the double-bounce scattering, the volume scattering, and the helix scattering model,

$$T = P_s T_{surface} + P_d T_{db\_bounce} + P_v T_{volume} + P_c T_{helix} \quad (1)$$

where P_s, P_d, P_v and P_c correspond to the power of each scattering mechanism. The Freeman-Durden Decomposition [1] assumes the volume scattering is the contribution from a cloud of randomly oriented dipoles, which follows the homogeneous distribution, such as in (2). The corresponding coherency matrix is in (3).

$$p(\theta) = \frac{1}{2\pi} \quad 0 \le \theta \le 2\pi \quad \text{with} \int_0^{2\pi} p(\theta) d\theta = 1 \quad (2)$$

$$T_{v\_uniform} = \frac{1}{4}\begin{bmatrix} 2 & 0 & 0 \\ 0 & 1 & 0 \\ 0 & 0 & 1 \end{bmatrix} \quad (3)$$

Based on the same assumption as in the Freeman Decomposition, Yamaguchi [2]-[3] extends the volume scattering model by introducing an additional distribution, as shown in (4). The corresponding two coherency matrices are in (5).

$$p(\theta) = \begin{cases} \frac{1}{2}\sin\theta & 0 < \theta < \pi \\ 0 & \pi < \theta < 2\pi \end{cases} \text{ with } \int_0^{2\pi} p(\theta) d\theta = 1 \quad (4)$$

$$T_{v\_\sin} = \frac{1}{30}\begin{bmatrix} 15 & 5 & 0 \\ 5 & 7 & 0 \\ 0 & 0 & 8 \end{bmatrix} or \frac{1}{30}\begin{bmatrix} 15 & -5 & 0 \\ -5 & 7 & 0 \\ 0 & 0 & 8 \end{bmatrix} \quad (5)$$

Both the double-bounce scattering and the surface scattering model are the same as those in Freeman's decomposition. After detailed analyses, it can be found that negative powers of the surface or the double-bounce scattering mechanism will definitely emerge, if and only if any one of the inequalities, shown in (6) and (7) in relation to the volume scattering models in (3) and (5), is satisfied.

$$\begin{cases} T_{11} < 2\left(T_{33} - \left|\mathrm{Im}\left(T_{23}\right)\right|\right) \\ T_{22} < T_{33} \\ \left|T_{12}\right|^2 > \left|T_{11} - 2\left(T_{33} - \left|\mathrm{Im}\left(T_{23}\right)\right|\right)\right| \cdot \left|T_{22} - T_{33}\right| \end{cases} \quad (6)$$

$$\begin{cases} T_{11} < 15\left(T_{33} - \left|\mathrm{Im}\left(T_{23}\right)\right|\right)/8 \\ T_{22} < T_{33} - \left(T_{33} - \left|\mathrm{Im}\left(T_{23}\right)\right|\right)/8 \\ T_{12}\ \text{m}5\left(T_{33} - \left|\mathrm{Im}\left(T_{23}\right)\right|\right)/8\right|^2 > \\ T_{11} - 15\left(T_{33} - \left|\mathrm{Im}\left(T_{23}\right)\right|\right)/8\right| \cdot \left|T_{22} - 7T_{33}/8 - \left|\mathrm{Im}\left(T_{23}\right)\right|/8\right| \end{cases} \quad (7)$$

Proc. 'Fringe 2011 Workshop', Frascati, Italy,
19–23 September 2011 (ESA SP-697, January 2012)

In addition, experimental results will indicate that the problem of overvaluation of the volume scattering power also exists in the Yamaguchi Decomposition, especially for those pixels in the urban areas. In the following section, an improved four-component decomposition method will be proposed to deal with the foregoing problems.

3. PROPOSED METHOD

3.1. Orientation Angle Compensation

The target orientation angle (OA) is the included angle between the SAR flying direction and the projection of the target on the SAR incidence plane. The geometry is illustrated in Fig. 1 (a) and (b). The orientation angle compensation (OAC) is to rotate the OA of the coherency matrix to zero by minimizing the power of the cross-polarization channel. That is equivalent to maximizing the power of the co-polarization channel. The OAC can be realized by different methods [4]-[5], whereas with the same compensation effects. The OAC algorithm [5] based on the 9 Huynen parameters is shown in Fig. 1 (c).

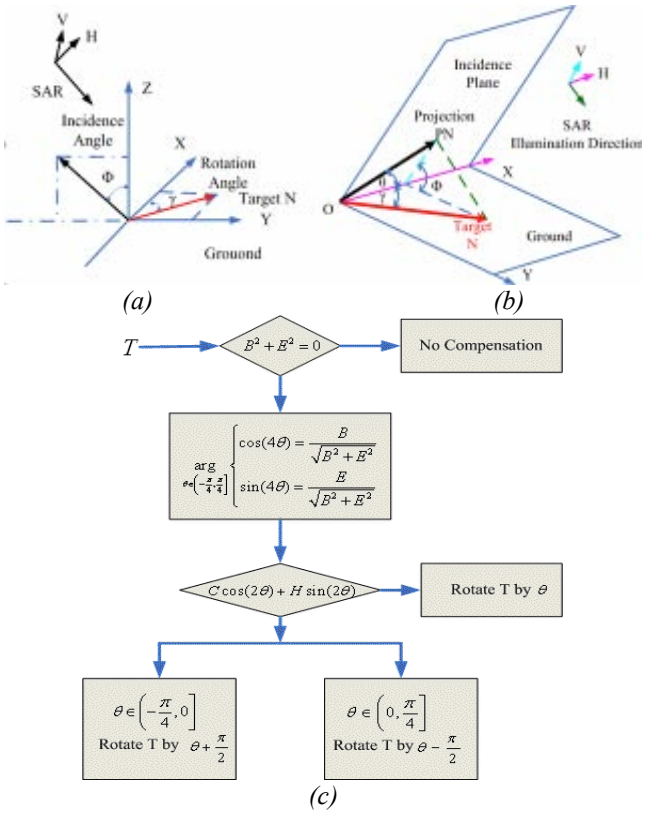

Figure 1. Orientation angle and flowchart of the OAC (a) Incidence geometry (b) sketch of the Orientation angle (c) flowchart of the OAC

In theory, the OAC disables the second inequality in (6) and (7), i.e., $T_{22} < T_{33}$ and $T_{22} < T_{33} - \left(T_{33} - \left|\mathrm{Im}\left(T_{23}\right)\right|\right)/8$. Additionally, as the helix power P_c is roll invariant, the OAC can bring down the volume scattering power P_v by reducing the value of T_{33}. It can also be easily observed that the number of pixels that meet the first and the third inequalities in (6) and (7) will decrease after the OAC.

3.2. Modified Volume Scattering Model

In the Freeman and Yamaguchi Decompositions, the cloud of randomly oriented dipoles is viewed as the contribution to the volume scattering. In view of the geometrical characteristics of tree trunks, branches, and leaves, it seems to be a suitable assumption for the densely vegetated areas.

However, the assumption of dipoles is not suitable to model the volume scattering mechanism in urban areas, because the geometrical shapes of the scatterers in urban areas are dissimilar to dipoles. Additionally, the volume scattering model based on the assumption of dipoles suffers from the overvaluation of volume scattering power for some specific buildings. Therefore, we propose to use a modified volume scattering model that can fit the scattering characteristics in the urban areas.

Suppose that such a basic scatterer has the scattering matrix as shown in (8). The uniform distribution is still applicable. Thus, the volume scattering model will be (9) and (10). Fig. 2 shows that different scattering mechanisms correspond to different values of ρ. Based on the assumption that pure volume scattering comes from pure randomness, we utilize the model with the maximum entropy, i.e. ρ=0, in our decomposition.

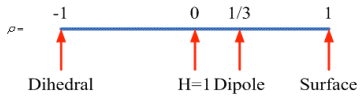

Figure 2. Volume scattering model with different parameters

Consequently, the volume scattering power is calculated as $3\left(T_{33} - P_c/2\right)$ in the proposed scheme, instead of $4\left(T_{33} - P_c/2\right)$ and $15\left(T_{33} - P_c/2\right)/4$. It is clear that the modified volume scattering model decreases the volume scattering power further.

$$S = \begin{bmatrix} S_{HH} & 0 \\ 0 & S_{VV} \end{bmatrix} \tag{8}$$

$$T_v = \frac{1}{3-\rho}\begin{bmatrix} 1+\rho & 0 & 0 \\ 0 & 1-\rho & 0 \\ 0 & 0 & 1-\rho \end{bmatrix} \tag{9}$$

with $$\rho = \frac{\left|S_{HH}\right|^2 + \left|S_{VV}\right|^2 + 6\,\mathrm{Re}\left(S_{HH}S_{VV}^*\right)}{3\left|S_{HH}\right|^2 + 3\left|S_{VV}\right|^2 + 2\,\mathrm{Re}\left(S_{HH}S_{VV}^*\right)} \tag{10}$$

3.3. Decomposition Flowchart

The flowchart of the proposed decomposition is in Fig. 3. As the OAC will show noisy results in the vegetated areas, we only conduct the OAC in the urban areas,

which are segmented by the H/A/α classification [6] at the beginning of the flowchart. The data should be filtered [7] to suppress the speckle and the negative powers caused by it.

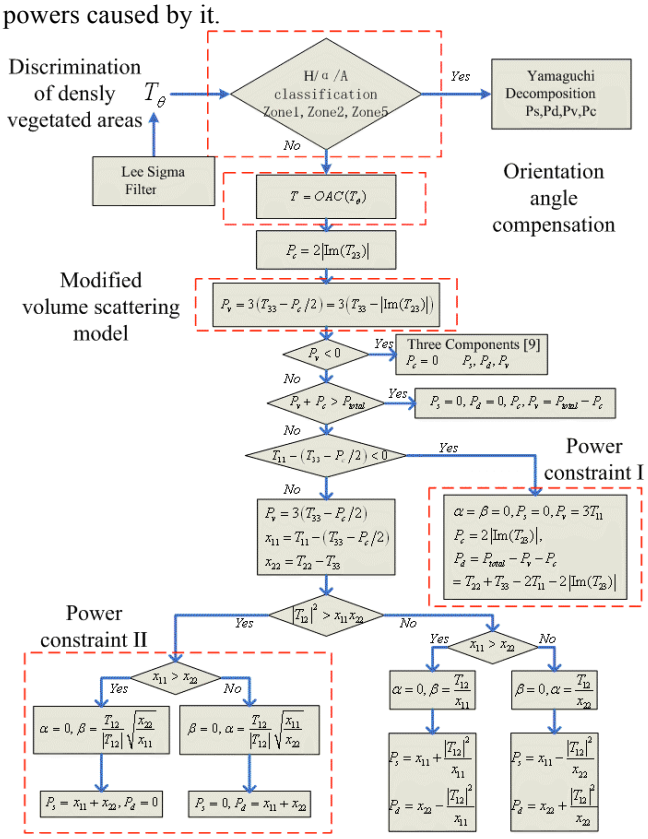

Figure. 3. Proposed decomposition scheme

We add two power constraints in the decomposition. The first one is to remove the negative powers caused by the first inequality in (6) and (7). The second one is applied to prevent the negative powers in P_d or P_s that caused by the third inequality in (6) and (7).

4. EXPERIMENTAL RESULTS

A RADARSAT-2 C-band quad polarimetric SAR image, acquired over the Suzhou City in China, is analyzed in the experiment. The imaging date is June 16, 2010. The image size is 778 × 728 pixels with 8 and 5 looks in the azimuth and the range directions, respectively. The original resolution is about 8 meters. The incidence angles in the near range and the far range are 38.37° and 39.85° , respectively. This scene includes extensive urban areas, farmlands and dense vegetation areas. Fig. 4 (a) is the Google Earth optical image. The span image of Suzhou City is shown in Fig. 4 (b).

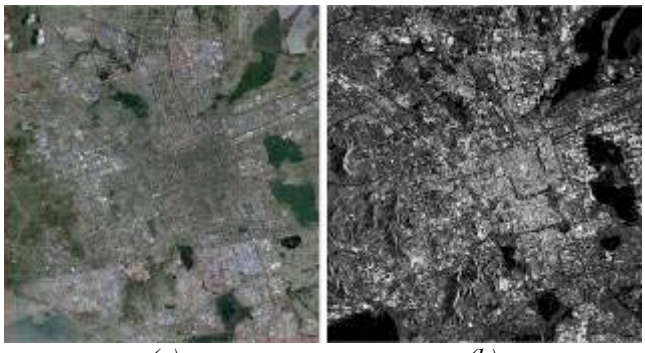

(a) *(b)*

Figure 4. Suzhou City, China
(a) Google Earth optical image ©2011, GeoEye (b) span image ©MacDonald, Dettwiler and Associates Ltd., 2010- All Rights Reserved

TABLE 1
EXPERIMENTS WITH NEGATIVE POWERS

Experiments	Pixels with negative powers
YD	74084
YD+OAC	15142
YD+OAC +MVSM[a]	3833
Proposed scheme	0

[a]YD, OAC, and MVSM are the abbreviations of the Yamaguchi Decomposition, the orientation angle compensation, and the modified volume scattering model, respectively.

As shown in Tab. 1, comparative experiments have been carried out and those pixels with negative powers are counted. In the experiments, all of the pixels in Zones 1, 2, and 5 in the H/A/α classification are excluded. Comparative decomposition results are exhibited in Fig. 5, where the image colours for the surface scattering power P_s, the double-bounce scattering power P_d, and the volume scattering power P_v are coded as blue, red, and green, respectively. Obviously, in Fig. 5 (a), many pixels in the urban areas are decomposed as "green" in the Yamaguchi Decomposition. Additionally, 74084 pixels with negative values in P_s or P_d emerge in the urban areas. The corresponding negative power map is shown in Fig. 5(d). Fig. 5(b) indicates that the overestimated volume scattering powers for quite a number of pixels in the urban areas are greatly suppressed by the OAC. For this reason, the pixels in the urban areas turn red. Moreover, the pixels with negative powers are also reduced by the OAC from 74084 in Fig. 5 (d) to 15142 in Fig. 5 (e). However, it can still be noted that quite a few pixels are coded as "yellow" in the urban areas in Fig. 5 (b), which demonstrates that the volume scattering power is still high, compared to the powers of other scattering mechanisms.

After utilizing the modified volume scattering model, these "yellow" pixels turn red, as is shown in Fig. 5 (c). Therefore, the pixels with negative powers are reduced further, from 15142 in Fig. 5 (e) to 3833 in Fig. 5 (f). As is shown in Tab. 1, after adding two power constraints in the proposed decomposition, the residual negative powers will be totally eliminated.

5. CONCLUSION

Experimental results verify the effectiveness of the three measures utilized in the proposed decomposition to eliminate the negative powers in the urban areas. The

overestimated volume scattering power in the urban areas is also suppressed efficiently in our method. Therefore, the Yamaguchi Decomposition is improved by the proposed scheme.

6. REFERENCES

1. Freeman, A. & Durden, S. L. (1998). A Three-Component Scattering Model for Polarimetric SAR Data. *IEEE Trans. Geosci. Remote Sens.*, vol. **36** (3), 963–973.
2. Yamaguchi, Y., Moriyama, T., Ishido, M. & Yamada, H. (2005). Four-Component Scattering Model for Polarimetric SAR Image Decomposition. *IEEE Trans. Geosci. Remote Sens.*, vol. **43** (8), 1699–1706.
3. Yamaguchi, Y., Yajima, Y. & Yamada, H. A Four-Component Decomposition of POLSAR Images Based on the Coherency Matrix. *IEEE Geosci. Remote Sens. Lett.*, vol. **3** (3), 292-296.
4. Xu, F. & Jin, Y. Q. (2005). Deorientation Theory of Polarimetric Scattering Targets and Application to Terrain Surface Classification. *IEEE Trans. Geosci. Remote Sens.*, vol. **43** (10), 2351–2364.
5. An, W., Cui, Y. & Yang, J. (2010). Three-Component Model-Based Decomposition for Polarimetric SAR Data. *IEEE Trans. Geosci. Remote Sens.*, vol. **48** (6), no. 6, 1667–1673.
6. Pottier, E. (1998). Unsupervised Classification Scheme and Topology Derivation of PolSAR Data Based on the H/ α /A Polarimetric Decomposition Theorem. in *Proc. 4th International Workshop on Radar Polarimetry*, Nantes, France, pp. 535–548.
7. Lee, J. S., Wen, J. H., Ainsworth, T. L., Chen, K. S. & Chen, A. J. (2009). Improved Sigma Filter for Speckle Filtering of SAR Imagery. *IEEE Trans. Geosci. Remote Sens.*, vol. **47** (1), 202–213.

ACKNOWLEDGMENT

This work was supported in part by the National Natural Science Foundation of China under Grants 40971198 and 40871191, and in part by the National High-Tech Research and Development Program of China under Grant 2009AA12Z118. The authors would like to thank Center for Earth Observation and Digital Earth of Chinese Academy of Sciences for providing the outstanding and well calibrated RADARSAT-2 quad polarization data, and the Google Corporation for providing the optical image with high resolution.

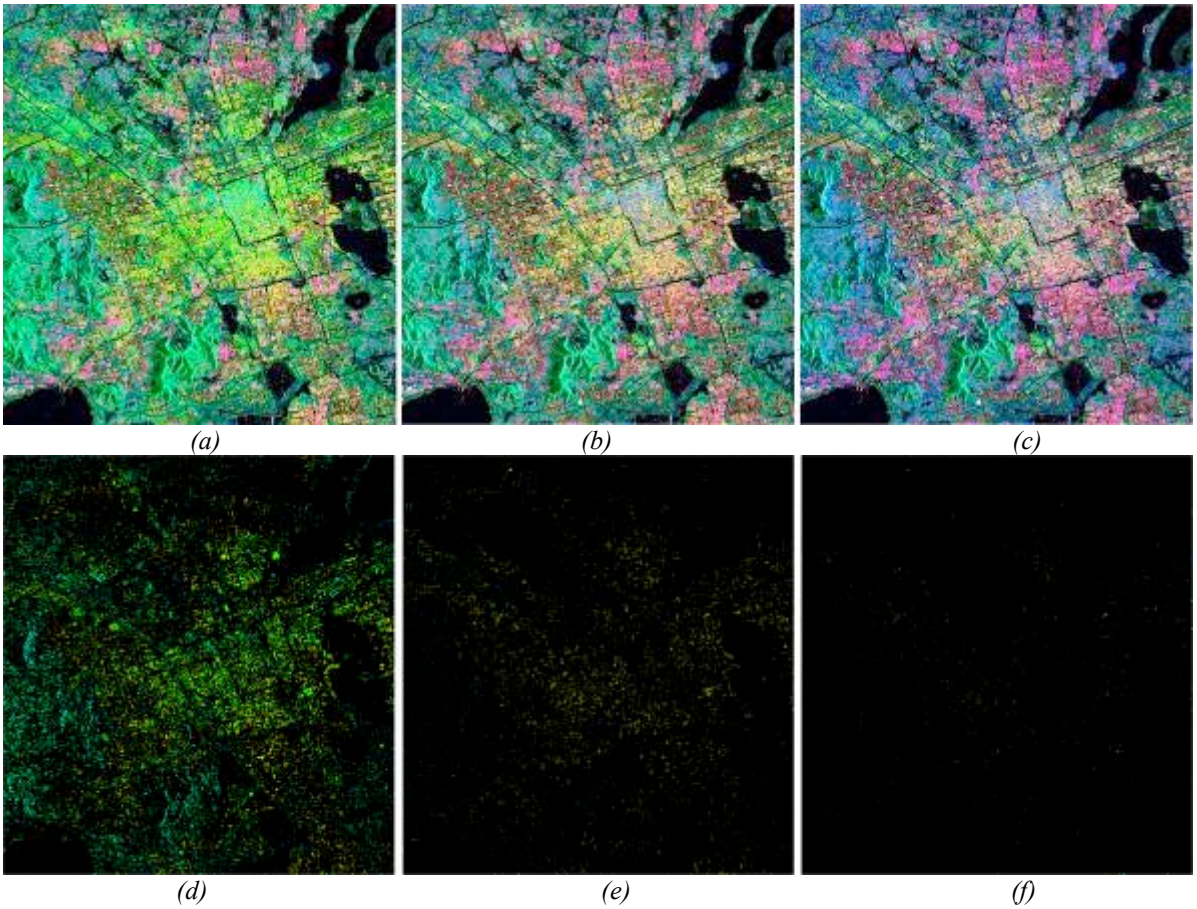

(a) (b) (c)

(d) (e) (f)

Figure 5. Comparison of decomposition results of the Radarsat-2 image © MacDonald, Dettwiler and Associates Ltd., 2010-All Rights Reserved (a) Yamaguchi (b) Yamaguchi+OAC (c) proposed scheme (d)(e)and (f) are negative power maps corresponding to (a)(b) and (c)